Cao, C., Diteesawat, R. S., Rossiter, J., & Conn, A. T. (2019). A Reconfigurable Crawling Robot Driven by Electroactive Artificial Muscle. In *IEEE International Conference on Soft Robotics (Robosoft 2019)* (pp. 840-845). [8722789] Institute of Electrical and Electronics Engineers (IEEE). https://doi.org/10.1109/ROBOSOFT.2019.8722789

A Reconfigurable Crawling Robot Driven by Electroactive Artificial Muscle

Chongjing Cao*, Richard Suphapol Diteesawat*, Jonathan Rossiter and Andrew T. Conn

***Abstract* — In nature, inchworms can move freely on uneven terrains where conventional wheeled or tracked robots cannot. Emerging soft actuation technologies such as dielectric elastomer actuators (DEAs) offer a new approach for inchworm-inspired robot designs thanks to their large actuation strain and inherent compliance. In this work, we present a reconfigurable inchworm-inspired crawling robot driven by DEAs that demonstrates two different crawling modes: vibrational crawling and two-anchor crawling. This modular design combines the advantages of fast speed through the vibrational crawling motion and payload transportation capability of the two-anchor crawling motion. A single vibrating module shows a fast locomotion speed of 0.9 body length / second. When two of the robot modules are configured into a two-anchor crawling mode, this new configuration can carry a payload of up to 35% its body weight at a slower speed.**

I. Introduction

Living organisms can often travel freely on uneven environment. For example, inchworms use a two-anchor gait to propel through various environments. This is done by alternately anchoring and releasing the front and rear legs while arching the body to propagate forward [1]. Inspired by this, many crawling robots have been developed in recent years which have potential for use in applications such as machine inspection, search-and-rescue, and minimally-invasive surgical robots. A common actuator for crawling robot designs is the shape-memory alloy (SMA) actuator which has large energy-density, large strain in coiled form and simple control [2]. For example, Trimmer and co-workers have developed a series of caterpillar-inspired robots driven by SMA actuators such as GoQBot [3], PS robot [4] and Softworms [5] which achieve locomotion by exploiting anisotropic friction. Dielectric elastomer actuators (DEAs) are an emerging type of soft actuator that have large actuation strains, high energy density, inherent compliance and low cost [6]. Several DEA driven inchworm robots have been developed. These include a pneumostatic two-segment inchworm robot with antagonistic DEA membranes [7], a multi-directional crawling robot with a planar multi-segment DEA and electroadhesion pads [8] and an annelid-inspired robot with multi-layer DEA diaphragms [9].

The crawling robots aforementioned control the displacement between the front and rear legs and utilize the frictional anisotropy to achieve a crawling gait and can be classed as 'two-anchor crawling'. On the other hand, a different approach is to utilize the frictional anisotropy of bristles in a 'vibrational crawling motion'. The general concept of such motion is to convert the vertical periodic oscillation of the robot into a forward motion using the asymmetric friction forces of the bristles. A vibratory motor (a DC motor driving an eccentric mass) is usually adopted as the excitation source, as has been shown in [10] [11] [12] [13]. These robots have the advantages of low-cost and are able to travel at a higher speed than two-anchor crawling robots (e.g. over 30 body length / second in [12]). However, the vibratory motors which have been used in previous vibrating crawling robots generate large noise.

In this work, we propose a reconfigurable modular soft robot design driven by DEAs that can be configured into both vibrational crawling and two-anchor crawling motions. This modular design combines the advantages of the fast speed of vibrational crawling motion and the payload transportation capability of the two-anchor crawling motion that are silent in operation and have the potential to ensure completely soft vibratory robots. A single robot module demonstrates a vibrational crawling by driving the DEA at its resonant frequency. When two or more of the robot modules are coupled together, the reconfigured robot can perform a two-anchor crawling. Figure 1 shows the robot prototype in vibrational crawling mode (a) and two-anchor crawling mode (b).

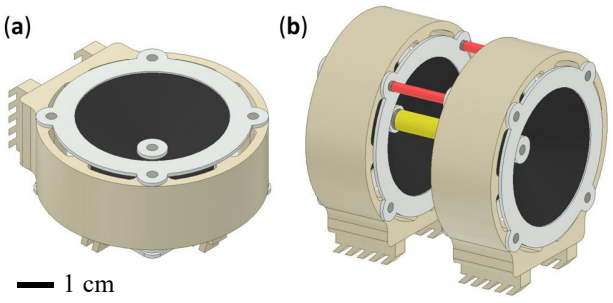

Figure 1. The proposed DEA-driven crawling robot prototype in (a) vibrational crawling mode and (b) two-anchor crawling mode.

This paper is structured as follows. In section II, the DEA design is introduced, and its quasi-static and dynamic performance are characterized. In section III, the locomotion concepts of both vibrational and two-anchor gaits are

C. Cao and R. S. Diteesawat are with Bristol Robotics Laboratory, University of Bristol and University of the West of England, BS16 1QY, UK (cc15716@bristol.ac.uk and richard.diteesawat@bristol.ac.uk).

* These authors contribute equally to this work.

J. Rossiter is with the Department of Engineering Mathematics, University of Bristol, BS8 1UB, UK.

A. T. Conn is with the Department of Mechanical Engineering, University of Bristol, BS8 1TR, UK.

explained, and the robot's design and fabrication process are reported. Experiments are conducted to characterize the velocity of the robot using both modes. Finally, discussion and conclusions are made in sections IV and V respectively.

II. Double Cone Dielectric Elastomer Actuator

A. DEA Design Overview and Fabrication

A double cone DEA configuration is adopted in this work for its simple structure, ease of fabrication and good stroke/force output [14] [15] [16]. This DEA design consists of two dielectric elastomer membranes bonded to rigid circular frames with an inner radius, b. A disk with a smaller radius, a, is bonded to the centre of each membrane. Compliant electrodes are added to the two sides of the membranes. The two frames are separated by a distance, h, while the central disks of the membranes are rigidly connected, as illustrated in Figure 2 (a). When passive, the two membranes exert equal forces and the central disks (end-effector) balance in the middle. When a voltage is applied across the electrodes of one membrane, the Maxwell pressure generated by the electric field induces planar expansion of the membrane, and the imbalance in force drives the end-effector. This principle is demonstrated in Figure 2 (b).

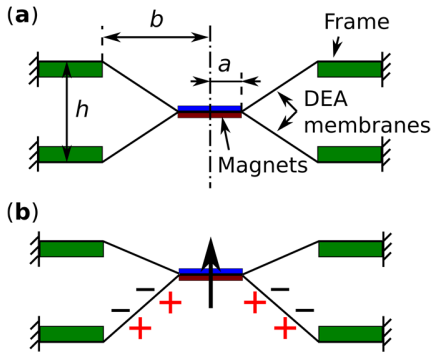

Figure 2. (a) Cross-sectional view of the double cone DEA. The central disks have radius, a, and the circular frames have inner radius, b. The two frames are separately by distance, h. (b) When a voltage is applied to one side of membrane, the end-effector is driven towards the opposite side.

The fabrication process of the DEA is described as follows. Silicone elastomer Elastosil (thickness 100 μm, Wacker Chemie AG) was used as the dielectric elastomer. The membranes were pre-stretched biaxially by 1.2 × 1.2 and then bonded to acrylic rings (b = 20 mm) using Sil-poxy (Smooth-On). Disk-shaped permanent magnets (0.1 g, a = 4 mm) were bonded to the centre of the membranes using Sil-poxy. The selected a/b ratio of 0.2 has been shown to have the best quasi-static output performance [17]. Carbon conductive grease (MG Chemicals) was hand-brushed on each side of the membranes as the compliant electrodes. The two membranes were separated using spacers and were oriented such that the opposite poles of the two magnets face each other on the two membranes, the attraction forces thereby coupling the two membranes in the centre. In our previous work, we have shown that the further the two membranes are separated, the stiffer the DEA becomes [16]. To find the optimal h value for this crawling robot application, four values were tested: h = 10, 15, 20 and 25 mm.

B. Quasi-static and Dynamic Characterization

The quasi-static and dynamic performance of the double cone DEA were characterized experimentally by varying height, h. First, the quasi-static force-stroke output was analysed. The fabricated DEA was fixed to the testing rig, an actuation voltage (V = 4380, 4220, 4040, 3820 V for h = 10, 15, 20, 25 mm respectively, which result in a same nominal electric field of E_n = 60 V/μm) was applied by a high voltage amplifier (Ultravolt, 5HV23-BP1) to one DE membrane, which resulted in a force-stroke output on the end-effector. A load cell (NO.1004, Tedea) was used to measure the blocking force F exerted by the DEA at the stroke d, and the load cell was moved away from the end-effector at a velocity of 0.01 mm/s by a linear rail (X-LSQ150B-E01, Zaber Technologies Inc.) until no force was measured. For each sample with different height h, measurements were repeated five times. Free actuation measurements were taken with a sine wave (amplitude = 4380, 4220, 4040, 3820 V for h = 10, 15, 20, 25 mm respectively) frequency sweep from 1 to 200 Hz and an increment of 0.1 Hz to characterize the dynamic performance of the DEA. A laser displacement sensor (LK-G152 and LKGD500, Keyence) measured the displacement of the end-effector. All experiments were controlled by MATLAB (MathWorks) and all data was collected by a DAQ device (National Instruments, BNC-2111) at a sampling frequency of 20,000 Hz.

Figure 3 (a) compares the quasi-static force-stroke relationship of the double cone DEA with heights of h = 10, 15, 20 and 25 mm. It can be seen that the force-stroke relationships for all four samples are approximately linear, which agrees with a previous double cone DEA study [15]. As h increases, the maximum blocking force that can be exerted by the DEA increases at the same nominal electric field, while the maximum stroke reduces. For two-anchor crawling, a larger blocking force output is preferred to overcome friction and to potentially carry heavier payloads. This suggests a DEA module with a larger height h is more suited for this mode.

The stroke of the double cone DEA with h = 20 mm against the excitation frequency is illustrated in Figure 3 (b). As the excitation frequency increases, two peaks can be observed in Figure 3 (b) where the second peak is the resonance of the DEA. The stroke at resonance is 5.5 mm, which is over ten times greater that at low frequencies (e.g. 1 Hz). Figure 3 (c) shows the resonant amplitude and the resonant frequency as a function of h. As h increases, the resonant amplitude reduces while the resonant frequency increases, which is due to the increasing membrane stiffness and has also been demonstrated in our previous study [16]. For vibrational crawling locomotion, increasing both oscillation amplitude and frequency can increase the velocity. As a result, by assessing both the quasi-static and dynamic performance, a height h = 20 mm is selected for our robot due to its good force-displacement output the maximum force amplitude during vibration ($F \propto A\omega^2$, where A is the amplitude of the DEA end-effector and ω is the resonant frequency).

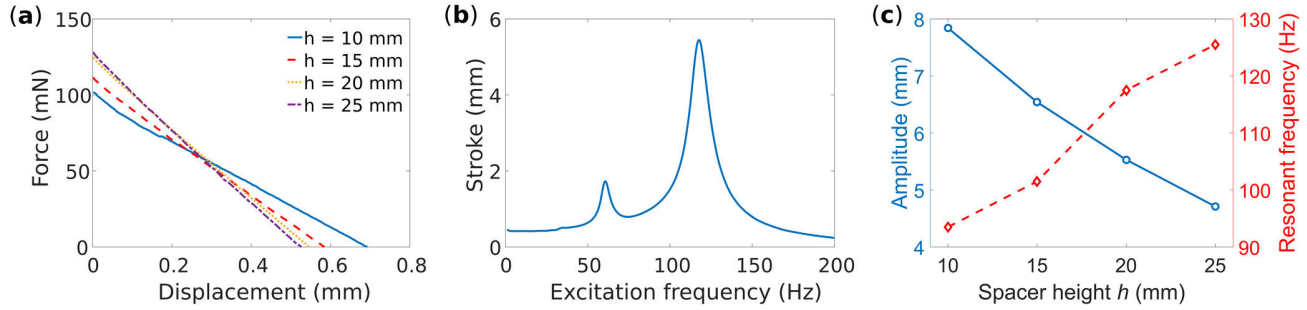

Figure 3. (a) Quasi-static force-stroke output of the double cone DEA with different heights, h. (b) Stroke as a function of the excitation frequency from 1 to 200 Hz of the double cone DEA with h = 20 mm. (c) Resonant amplitude and resonant frequency of the double cone DEA as a function of height, h.

III. Reconfigurable Crawling Robot

A. Locomotion Principles

The locomotion principle for the vibrational crawling mode is illustrated in Figure 4 (a). In this mode, the robot is excited by a harmonic oscillating mass that is driven vertically by the double cone DEA at its resonance. The bristles can be modelled as rigid legs connected to the robot body via torsional springs. In one cycle, as the mass oscillates downward then upwards, normal forces F_{N1} and F_{N2} ($F_{N1} > F_{N2}$) are exerted consecutively on the bristles with corresponding friction force F_{f1} and F_{f2}. Due to the anisotropic friction coefficients in forwards and backward directions, F_{f2} is smaller than F_{f1}, leading to a forward displacement dx in one cycle.

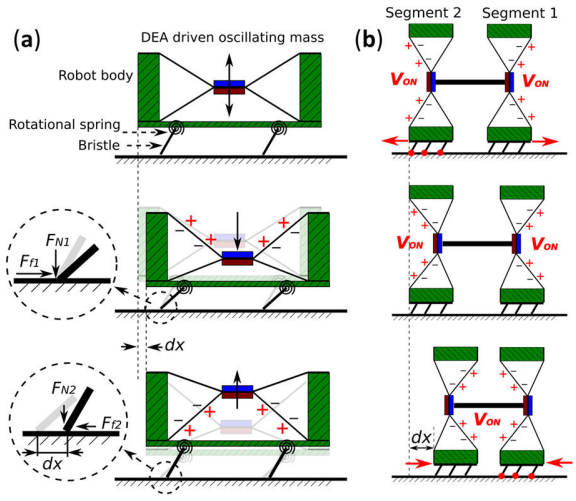

Figure 4. (a) Locomotion principle of the vibrational crawling mode. (b) Locomotion principle of the two-anchor crawling mode.

In the two-anchor crawling mode, the same principle of anisotropic friction principle is also utilized, but with two robot segments. Each segment is placed orthogonally to the ground such that the double cone DEA actuates parallel to the ground. The two segments are coupled with a rigid rod attached to the end-effectors of the DEAs. As illustrated in Figure 4 (b), when the two DE membranes on the outside are actuated, the distance between the two segments increases and Segment 1 is pushed forward while Segment 2 remains stationary due to the anisotropic friction on the bristles. The two segments are then driven towards each other by actuating the DE membranes on the inside. Now Segment 1 anchors while Segment 2 is pulled forward. The robot travels a forward distance dx in one actuation cycle.

B. Robot Design and Fabrication

A single robot module consists of three main parts: a double cone DEA, a soft robot body and bristles as demonstrated in Figure 5 (a). All components are connected to each together via magnets, which allows easy assembly and disassembly and reduces the complexity in fabrication. Individual DEA frames are attached to the top and the bottom of the robot body; their central disks are connected via magnets. Two long bristles are connected to the flat surface on the robot body for two-anchor crawling mode and four short bristles were attached to the bottom of the robot body for vibrational crawling. For the two-anchor crawling mode, two modules are placed orthogonally to the ground and are coupled via a plastic core at the central disks of the DEAs and two plastic rods on the top of the robot body, as illustrated in Figure 5 (b). These rods connect the two segments of the robot to perform two-anchor crawling.

The soft robot body has a cylinder shape with an outer radius of 30 mm and a wall thickness of 2.5 mm. One side was modified to form a 37 mm wide flat surface for attaching bristles. The height of the body was set to be 20 mm to ensure the optimal double cone DEA height of h = 20 mm as discussed in Section II. Four 18 mm long plastic rods with magnets (radius = 1.5 mm, thickness = 1.0 mm) at both ends were inserted in the robot body to reinforce the structure. DEAs with the size of a = 4 mm and b = 20 mm were bonded to 1 mm thickness acrylic circular frames with an outer radius of 26 mm using the method as described in Section II.A. Bristles were attached to the robot body by Sil-poxy (Smooth-On). The soft robot body and bristles were made of PDMS (Sylgard 184, DOWSIL), and the fabrication process is described as follow. First, acrylic moulds were laser-cut and stacked together. PDMS was mixed with the hardener with the weight ratio of 10:1 and placed in a vacuum chamber for 10 minutes. To visualize the clear PDMS structure better, luminescent pigment was also added to the PDMS during the mixing process. Then PDMS was poured into the moulds and placed in a 40˚C oven for 48 hours. Finally, the cured robot body and bristles were removed from the moulds and assembled. Each fabricated robot module including DEAs weights 26 g.

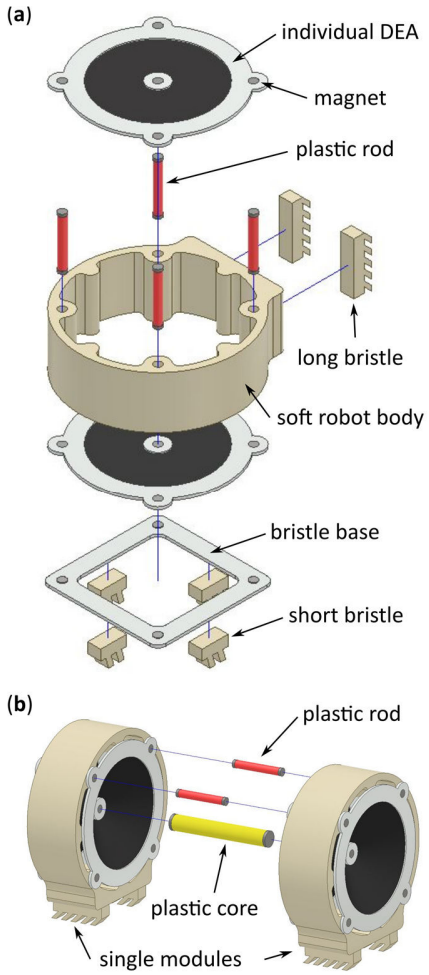

Figure 5. (a) Exposed view of one robot module. (b) Two modules assembled.

C. Bristle Angle Characterization

The two-anchor crawling mode of the robot depends on the anisotropic friction of the bristle. A higher backward to forward friction ratio is essential for a robust two-anchor gait. In this section we compare the backward to forward friction ratio of the bristles with varied tilting angles from $\alpha = 0^\circ$ to 45°. The bristle parameters are demonstrated in Figure 6 (a). The experimental setup for bristle characterization is described as follows. Each bristle sample was rigidly connected to a linear rail (X-LSQ150B-E01, Zaber Technologies Inc.) and was placed on top of an acrylic plate. The linear rail moved the bristle relative to the acrylic plate in forward and backward directions at a velocity of 0.1 mm/s while the friction force was measured by a load cell (NO. 1004, Tedea). Each experiment was repeated five times and the results were averaged. Figure 6 (b) shows the measured backward to forward friction ratios for bristles with tilt angles from 0° to 45°. As can be seen, the friction ratio increases to over 4 when the tilt angle is at 45°. A larger tilt angle was not included in this study due to the increasing difficulty in the moulding fabrication process.

The large friction ratio at 45° shows that this angle is the best tested value in this study for the two-anchor crawling mode. However, as previous studies have suggested [18], a large bristle tilt angle can reduce the speed for vibrational crawling motion, hence in our design, 45° is only selected for two-anchor crawling mode, while the best angle for vibrational crawling mode will be investigated in the next section.

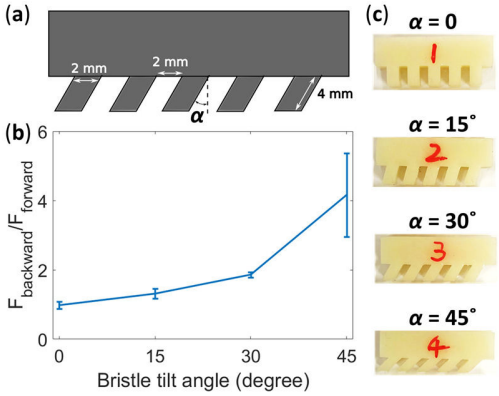

Figure 6. (a) Bristle design parameters. (b) Backward to forward friction ratio $F_{backward}/F_{forward}$, as a function of bristle tilt angle α from 0° to 45°. (c) Fabricated bristles.

D. Locomotion Experiments

1) Vibrational crawling

The vibrational crawling mode was tested with different bristle angles on a flat surface (smooth acrylic plate). Two AC sine actuation waves with the amplitude of 4040 V and 180° out-of-phase were applied to the two DE membranes to create oscillation. The resonant frequency of the DEA was measured at 124 Hz. The experiments were recorded by a camera (Panasonic DMC-G80) at a frame rate of 25 fps and the velocity was estimated by tracking a marker on the robot using a custom motion tracking script in MATLAB. All experiments were repeated five times.

The measured velocity of the vibrational crawling mode against the bristle tilt angle is plotted in Figure 7. As it can be seen, the velocity reduces with the increasing bristle angle. At the bristle angle of 15°, a peak velocity of 55 mm/s (0.9 body length/s) was obtained with a power consumption of approximately 20 mW. As a result, a bristle angle of 15° was determined for the vibrational crawling mode in the final robot prototype. Figure 8 shows a series of frames of the single robot module in vibrational crawling. It should be noted that due to the transparent nature of the PDMS material, in order to better visualize the locomotion of the robot, ultraviolet lighting with a dark background was used for robot demonstrations.

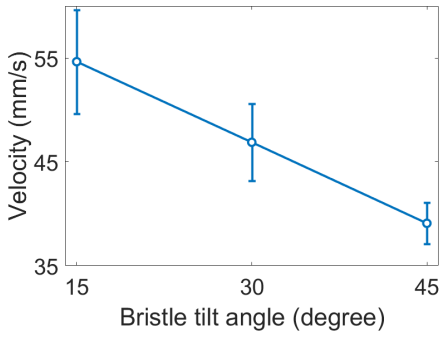

Figure 7. Velocity in vibrational crawling mode against bristle tilt angle.

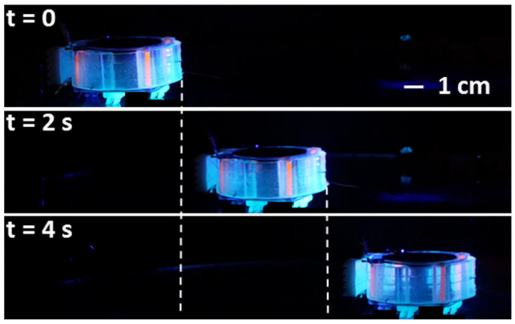

Figure 8. Vibrational crawling motion of the robot at 124 Hz actuation frequency (side view). (video online: https://youtu.be/hskzyLLVr7g)

2) Two-anchor Crawling

The two-anchor crawling mode was tested with different actuation frequencies. Two layers of Elastosil were used for each DEA membrane in this mode to increase the blocking force output and overcome the forward friction force, $F_{forward}$. Two square wave AC voltages with the amplitude of 4040 V and the phase shift of 180˚ were applied with the frequencies of 2 to 40 Hz. Figure 9 (a) compares the velocity and the stride (displacement per cycle) of two-anchor crawling as a function of the actuation frequency. The velocity increases with the increasing frequency and reaches a peak of 6.6 mm/s (0.1 body length / s) at 35 Hz and then drops sharply at 40 Hz due to the insufficient charging and discharging of the DEAs (a limitation of the high voltage supplies and electrodes). The maximum speed is comparable with other DEA crawling robots (0.05 and 0.1 body length / s in [7] and [8] respectively). At 35 Hz where the velocity is the highest, the power consumption is approximately 300 mW. The displacement of the front segment of the robot as a function of time at 2 Hz crawling is shown in Figure 9 (b). As can be seen, at the start of one cycle, the front segment first slides forward, then as the rear segment moves forward, the front segment slides backward due to the reaction force. However, because of the anisotropic friction, the robot generates a net forward displacement in one complete cycle. The stride fluctuates as the actuation frequency increases and shows a peak of 0.25 mm at the frequency of 20 Hz. At frequencies from 20 Hz to 35 Hz, the stride reduces even though the crawling velocity increases continuously. By comparison, a maximum stride of 0.44 mm was achieved in vibrational crawling mode.

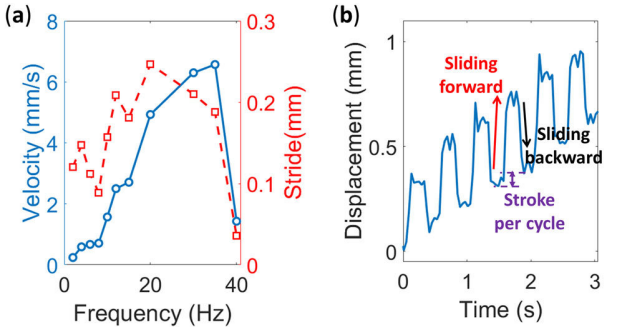

Figure 9. (a) Velocity and stride in two-anchor mode against actuation frequency. (b) Displacement of the robot in 2 Hz crawling.

Figure 10 (a) demonstrates a series of frames of the two robot modules coupled to achieve two-anchor crawling mode at an actuation frequency of 35 Hz. To demonstrate the payload transportation capability using two-anchor mode, two 10 g weights were placed on the robot, which is equivalent to 35% of the robot's body weight. The robot was able to achieve a speed of 0.09 mm/s, as is shown in Figure 10 (b).

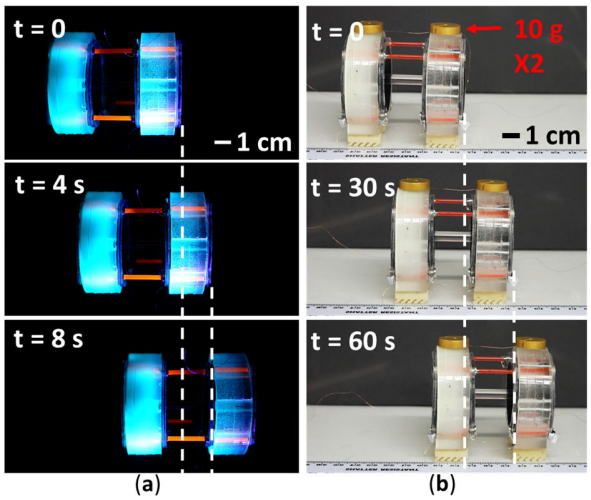

Figure 10. (a) Two-anchor crawling motion at 35 Hz actuation frequency (top view). (b) Two-anchor crawling motion with 20 g payload (side view).

IV. Discussion

The current crawling robot design demonstrates the potential of applying this reconfigurable modular soft robot in both vibrational crawling and two-anchor crawling motions. A higher velocity with a lower power consumption was demonstrated using vibrational crawling mode, which resulted in a significantly lower cost of transport (COT) of 1.35 than 77.3 in two-anchor crawling mode (COT = P/mgv, where P is the power consumption, m is the mass of the robot (weight of the power supply is not considered here), g is gravitational acceleration, v is the transport velocity). The low COT allows this robot to travel a greater distance with the same amount of energy in vibrational crawling mode. In two-anchor mode, the current prototype was able to travel with a payload 35% of its body weight. The major contribution of this work is the development of a reconfigurable robot which allows adjustment of the locomotion mode only by reconfiguring the robot to adapt to different scenarios where either fast speed or payload transportation is required.

Several improvements can be made to increase the locomotion speed. For the double cone DEA, the pre-stretch ratio of the membranes and the mass attached to the DEA can be optimized in order to obtain a large periodical oscillation force on the robot at a higher frequency. Currently, carbon grease was adopted as the DEA electrodes, which increases the viscoelasticity of the actuator and the high electrical resistance and the low power input of the high voltage supply (< 1 W) restricts the performance of the DEA at its resonance. In the future work, electrodes with higher conductivity such as carbon nanotubes [19] can be adopted with novel pattern techniques such as inkjet printing [20]. For both vibrational and two-anchor crawling, increasing the number of layers of the DE membranes can multiply the blocking force output and the power output of the actuator hence increasing the speed

and payload carrying capability. Structural optimization can be developed to reduce the weight of the robot, which leads to a lower friction on the bristle thus increasing the crawling speed. The current prototype can only achieve a forward crawling in both vibrational and two-anchor crawling, but in the future development, a steering mechanism for two-anchor crawling is proposed which takes advantage of the multi-degree-of-freedom double cone DEAs [14] [15] [21]. For steering in vibrational crawling, different resonant modes of the DEA can be utilized, which generate directional forces, as has been demonstrated by [22]. To achieve real applications of such reconfigurable robot in rescue and surveillance using either swarm vibrational crawling or assembled worm configuration crawling, on-board power supply as well as control systems must be developed. With the advancement in power electronics and battery technologies, several untethered DEA robots have been developed, such as [23] [24], proving the feasibility of developing small scale untethered DEA driven robots. The attachment and detachment of the modules in current prototype was achieved manually, but in the future work, a self-reconfigurable robot can be developed by using fast transfer of angular momentum in the body of each module to perform attachment and detachment, as has been demonstrated by [25].

V. Conclusion

In this work, we have presented a soft reconfigurable robot driven by soft DEAs that exhibits a fast vibrational crawling mode of a single robot module and a two-anchor crawling in an assembled configuration. At low actuation frequencies, the double cone DEA exerts force to overcome the friction and achieve two-anchor crawling. At its resonant frequency, the large oscillation amplitude allows a vibrational crawling motion. Experiments showed the performance of the DEA can be optimized by adjusting the gap between the two DE membranes. As the key towards achieving frictional anisotropy, the bristle tile angle was found to have different optimal values for two-anchoring crawling (45˚) and vibrational crawling (15˚). The final prototype showed a peak speed of 55 mm/s (equal to 0.9 body length / s) in vibrational crawling mode and 6.6 mm/s (0.1 body length /s) in two-anchor crawling mode. A payload transport capability of up to 35% its body weight was demonstrated using two-anchor mode. This novel reconfigurable soft robot combines the advantage of low cost of transport in the vibrational crawling mode and the capability of transferring payload in the two-anchor crawling mode and can potentially be used in applications such as disaster response where broad area searching and payload transportation are required.

Acknowledgment

This work was supported by the EPSRC Centre for Doctoral Training in Future Autonomous and Robotic Systems (FARSCOPE, grant EP/L015293/1) at the Bristol Robotics Laboratory where CC and RSD are PhD students. JR was supported by EPSRC grants EP/M020460/1 and EP/M026388/1 and was also funded by the Royal Academy of Engineering as a Chair in Emerging Technologies. AC acknowledges the support by EPSRC grant EP/P025846/1.

References

[1] L. Van Griethuijsen and B. Trimmer, "Locomotion in caterpillars," Biological Reviews, vol. 89, no. 3, pp. 656-670, 2014.
[2] T. Duerig, K. Melton and D. Stöckel, Engineering aspects of shape memory alloys, Butterworth-Heinemann, 2013.
[3] H. Lin, G. Leisk and B. Trimmer, "GoQBot: a caterpillar-inspired soft-bodied rolling robot," Bioinspiration & Biomimetics, vol. 6, no. 2, p. 026007, 2011.
[4] T. Umedachi, V. Vikas and B. Trimmer, "Highly deformable 3-d printed soft robot generating inching and crawling locomotions with variable friction legs," in 2013 IEEE/RSJ International Conference on Intelligent Robots and Systems (IROS), Tokyo, 2013.
[5] T. Umedachi, V. Vikas and B. Trimmer, "Softworms: the design and control of non-pneumatic, 3D-printed, deformable robots," Bioinspiration & Biomimetics, vol. 11, no. 2, p. 025001, 2016.
[6] R. Pelrine, R. Kornbluh, Q. Pei and J. Jose Joseph, "High-Speed Electrically Actuated Elastomers with Strain Greater Than 100%," Science, pp. 836-839, 2000.
[7] A. Conn, A. Hinitt and P. Wang, "Soft segmented inchworm robot with dielectric elastomer muscles," in Electroactive Polymer Actuators and Devices (EAPAD), 2014.
[8] K. Digumarti, C. Cao, J. Guo, A. Conn and J. Rossiter, "Multi-directional Crawling Robot with Soft Actuators and Electroadhesive Grippers," in IEEE International Conference on Soft Robotics (RoboSoft), 2018.
[9] K. Jung, J. Koo, Y. Lee and H. Choi, "Artificial annelid robot driven by soft actuators," Bioinspiration & Biomimetics, vol. 2, no. 2, p. 42, 2007.
[10] Y. Han, H. Marvi and M. Sitti, "Fiberbot: A miniature crawling robot using a directional fibrillar pad," in IEEE International Conference on Robotics and Automation (ICRA), Seattle, 2015.
[11] F. Becker, S. Boerner, V. Lysenko, I. Zeidis and K. Zimmermann, "On the mechanics of bristle-bots-modeling, simulation and experiments," in 41st International Symposium on Robotics, 2014.
[12] L. Giomi, N. Hawley-Weld and L. Mahadevan, "Swarming, swirling and stasis in sequestered bristle-bots," Proc. R. Soc. A, vol. 469, no. 2151, p. 20120637, 2013.
[13] K. Djen, H. Tim and R. Jonathan, "Kinematic analysis of vibrobot: a soft, hopping robot with stiffness-and shape-changing abilities," Frontiers in Robotics and AI, vol. 3, p. 60, 2016.
[14] H. Choi, K. Jung, J. Kwak, S. Lee, H. Kim, J. Jeon and J. Nam, "Digital polymer motor for robotic applications," in ICRA'03. IEEE International Conference on, 2003.
[15] A. Conn and J. Rossiter, "Antagonistic dielectric elastomer actuator for biologically-inspired robotics," in Electroactive Polymer Actuators and Devices (EAPAD), 2011.
[16] C. Cao, S. Burgess and A. Conn, "Flapping at resonance: Realization of an electroactive elastic thorax," in IEEE International Conference on Soft Robotics (RoboSoft), 2018.
[17] C. Cao and A. Conn, "Performance Optimization of a Conical Dielectric Elastomer Actuator," Actuators, vol. 7, no. 2, p. 32, 2018.
[18] N. Koumakis, A. Gnoli, C. Maggi, A. Puglisi and R. Di Leonardo, "Mechanism of self-propulsion in 3D-printed active granular particles," New Journal of Physics, vol. 18, no. 11, p. 113046, 2016.
[19] M. Duduta, D. Clarke and R. Wood, "A high speed soft robot based on dielectric elastomer actuators," in IEEE International Conference on Robotics and Automation (ICRA), Singapore, 2017.
[20] D. McCoul, S. Rosset, S. Schlatter and H. Shea, "Inkjet 3D printing of UV and thermal cure silicone elastomers for dielectric elastomer actuators," Smart Materials and Structures, vol. 26, no. 12, p. p125022, 2017.
[21] A. Conn and J. Rossiter, "Towards holonomic electro-elastomer actuators with six degrees of freedom," Smart Materials and Structures, vol. 21, no. 3, p. 035012, 2012.
[22] C. Tang, B. Li, H. Fang, Z. Li and H. Chen, "A speedy, amphibian, robotic cube: Resonance actuation by a dielectric elastomer," Sensors and Actuators A: Physical, vol. 270, pp. 1-7, 2018.
[23] T. Yang, Y. Xiao, Z. Zhang, Y. Liang, G. Li, M. Zhang, S. Li, T. Wong, Y. Wang, T. Li and Z. Huang, "A soft artificial muscle driven robot with reinforcement learning," Scientific reports, vol. 8, no. 1, p. 14518, 2018.
[24] T. Li, G. Li, Y. Liang, T. Cheng, J. Dai, X. Yang, B. Liu, Z. Zeng, Z. Huang, Y. Luo and T. Xie, "Fast-moving soft electronic fish," Science Advances, vol. 3, no. 4, p. 1602045, 2017.
[25] J. Romanishin, K. Gilpin and D. Rus, "M-blocks: Momentum-driven, magnetic modular robots," in IEEE/RSJ International Conference on Intelligent Robots and Systems (IROS), 2013.